

# ELECTROMAGNETIC FLOW CONTROL IN THE RIBBON GROWTH ON SUBSTRATE (RGS) PROCESS

BECKSTEIN P., GALINDO V., GERBETH G.  
 Helmholtz-Zentrum Dresden-Rossendorf (HZDR)  
 Bautzner Landstraße 400, 01328 Dresden, Germany  
 E-mail: [p.beckstein@hzdr.de](mailto:p.beckstein@hzdr.de)

The Ribbon Growth on Substrate (RGS) technology promises a very efficient approach for future photovoltaic (PV) silicon wafer production compared to the majority of commonly accepted processes. Although, for an eventual break-through of this RGS technology a number of remaining problems need to be addressed to increase process stability. We have therefore performed numerical investigations in order to study the influence of the involved AC magnetic fields on the silicon melt during the RGS process.

## 1. Introduction to the RGS process

Photovoltaic silicon is today mainly produced by directional solidification of multi-crystalline silicon or by the Czochralski growth method of silicon single crystals. Wafers are then obtained by sawing the ingots. The unavoidable sawing losses of prevalent processes are still in the range of 40...50% of the fed material. One very efficient way to avoid this deficit in terms of energy and material is the Ribbon Growth on Substrate (RGS) technology, which was suggested and developed during the last decade [1, 2].

The basic idea of this process is a continuous feeding of molten silicon into a casting frame without bottom, while a solidified silicon foil is extracted sidewise on a sub-cooled moving substrate underneath. Figure 1 shows a schematic of this principle. This brings both a close to perfect material yield by avoiding sawing losses, and a low energy consumption due to the continuous nature of the processing. Nearly all of the silicon melt is directly used to form the wafer itself. Another distinct advantage of the RGS process also comes from its fully decoupled solidification and casting velocity.

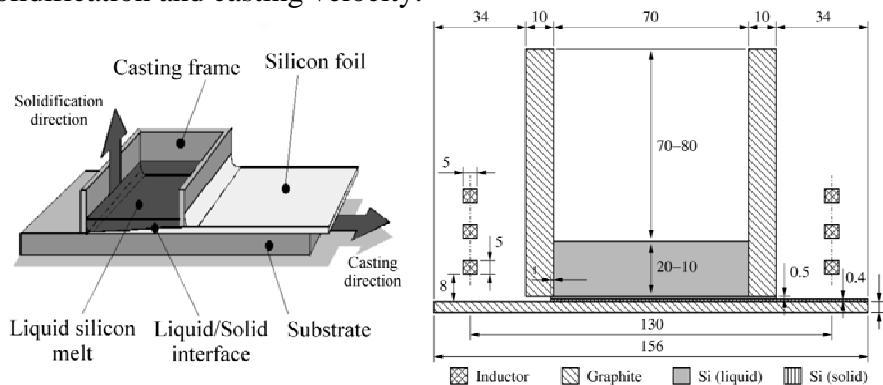


Figure 1: Scheme of the RGS process without excitation coils (left, [1]) and the simplified numerical model geometry (right, dimensions in mm). The drawing on the right represents both a central longitudinal section of the actual 3D-model and a derived 2D-version of the full model.

One challenging task in realizing this idea technically is the need to fully control the liquid silicon outflow. On this account, AC magnetic fields are applied to counter the gravitational forces acting on the melt, without contact. The excitation coil which is therefore utilized provides both a kind of magnetic valve and an inductive heating of the casting frame. The former actively prevents leakage in the slit regions and reduces wave-like oscillations at the extraction front of the silicon foil through electromagnetic forces. This valve only works because of capillarity effects in the slit regions based on the strong surface tension of the melt.

Recent activities on electromagnetic retention for liquid silicon have been reported in [3]. A leading problem which still has to be addressed is the occurrence of flow instabilities and meniscus oscillations at the open slits where the moving substrate enters and leaves the casting frame.

We show in this paper that it is generally possible to selectively influence the process by means of tailored magnetic fields. Based on simplified numerical simulations we demonstrate the effect of the applied AC magnetic fields on the silicon melt in the RGS process, taking into account the strong time-dependent coupling to the flow in the melt. The model which was used for this analysis is shown in Figure 1 (right). Part of the numerical investigation is devoted to the effect of different coil system geometries on the stress balance along the slit. Moreover, as the induction coil frequency is sensitive to the circuit load, the induction's dependency on the filling level was of considerable interest for sensing purposes.

## 2. Modelling overview

A typical associated process parameter set, which evolved mainly from empirical analysis, is a RMS-current of  $I_{RMS} = 1000 \text{ A}$  at a frequency of  $f = 10 \text{ kHz}$  to feed the excitation coils, in combination with a substrate velocity of  $u_s = 1 \text{ m/s}$ . The most important properties of involved materials, as shown in Figure 1 (right), are listed in Table 1.

Material	$\rho \left[ \frac{\text{kg}}{\text{m}^3} \right]$	$\eta \text{ [Pa} \cdot \text{s]}$	$\sigma \left[ \frac{\text{S}}{\text{m}} \right]$	$\gamma \left[ \frac{\text{N}}{\text{m}} \right]$	$\delta \text{ [mm]}$
Liquid silicon	2580	$0.86 \times 10^{-3}$	$1.20 \times 10^6$	0.733	5.0
Solid silicon	2540	-	$8.30 \times 10^4$	-	17.0
Graphite	1880	-	$1.25 \times 10^5$	-	14.0
Copper	8960	-	$6.00 \times 10^7$	-	0.7

Table 1: Material properties for different materials: Density  $\rho$ , kinematic viscosity  $\eta$ , electrical conductivity  $\sigma$ ,

surface tension coefficient  $\gamma$  and skin depth  $\delta = \sqrt{\frac{1}{\pi f \mu_0 \sigma}}$  assuming a frequency of 10 kHz.

A comprehensive RGS-model has to correctly represent a fully three-dimensional and two-way-coupled system of AC magnetic fields and fluid flow with free surfaces at the slit and at top of the melt in the crucible for those material values presented above.

The magnetic fields may be described using the  $\mathbf{A}$ - $V$ -formulation of the Maxwell-Equations implying MHD approximations, a small Magnetic Reynolds Number and no magnetization as:

$$\mathbf{B} = \nabla \times \mathbf{A}; \quad \mathbf{E} = -(\partial_t \mathbf{A} + \nabla V); \quad \frac{\|\mathbf{u} \times \mathbf{B}\|}{\|\mathbf{E}\|} \ll 1 \quad (1)$$

Here the velocity field is denoted by  $\mathbf{u}$ , the time by  $t$ . Taking the magnetic vector potential  $\mathbf{A}$  with applied Coulomb-Gauge and the electric scalar potential  $V$  instead of the magnetic  $\mathbf{B}$  and electric field  $\mathbf{E}$  allows us to explicitly introduce a source current density  $\mathbf{j}_s(t_{RMS})$  term into the system which represents the effect of the excitation coil [4]. In case of a constant ( $\nabla \sigma = \mathbf{0}$ ) or even zero ( $\sigma \equiv \mathbf{0}$ ) electrical conductivity it can be shown [5], that the scalar potential may simply be neglected if  $\mathbf{A}$  is conceptually substituted with a modified version:  $\hat{\mathbf{A}} = \mathbf{A} - \int \nabla V dt$ . That is, if we imply constant  $\sigma$  for each material only  $\mathbf{A}$  is required:

$$\nabla \times \nabla \times \mathbf{A} + \sigma \mu_0 \partial_t \mathbf{A} = \mu_0 \mathbf{j}_s; \quad \nabla \cdot \mathbf{A} = 0 \quad (2)$$

$$\mathbf{j} = \mathbf{j}_i + \mathbf{j}_s, \quad \mathbf{j}_i = -\sigma \partial_t \mathbf{A} \quad (3)$$

The field  $\mathbf{j}_i$  represents the induced current density. To find suitable boundary conditions, the numerical domain is divided into several regions with constant  $\sigma$ . A detailed mathematical

description of all the boundary conditions can also be found in [4]. By introducing complex-valued sinusoidal fields, equations **Error! Reference source not found.** to **Error! Reference source not found.** can be transformed into their frequency domain for an angular frequency of  $\omega = 2\pi f$ . This approach leads to a stationary problem since the time derivatives may then

be substituted with a complex-valued angular frequency ( $\frac{\partial}{\partial t} = i\omega$ ). For the momentum

balance of the fluid, only the time-averaged Lorentz force  $f = \frac{1}{\rho} \mathbf{j} \times \mathbf{B}_t$  is important. The fluid dynamics describing the silicon melt flow is governed by the principle of conservation of mass and momentum. For the RGS-model this leads to the incompressible Navier-Stokes-Equation [6] with additional terms for gravity and the time-averaged Lorentz-Force as described above:

$$\rho[\partial_t \mathbf{u} + (\mathbf{u} \cdot \nabla) \mathbf{u}] = \nabla \cdot \boldsymbol{\tau} + \rho \mathbf{g} + \langle \mathbf{j} \times \mathbf{B}_t \rangle; \quad \nabla \cdot \mathbf{u} = 0 \quad (4)$$

$$\boldsymbol{\tau} = \eta[\nabla \mathbf{u} + (\nabla \mathbf{u})^T] - p \mathbf{I} \quad (5)$$

Here  $\boldsymbol{\tau}$  represents the total stress tensor including the diagonal fluid pressure  $p$ . Surface tension is only acting on free surface boundaries. It is thereby worth to mention that the viscosity of the external atmosphere, which is in contact with the liquid melt at the conductor boundary, is several orders of magnitude smaller than the viscosity of the melt itself. Thus, the fluid boundary condition at the free surface with its outward unit normal  $\mathbf{n}$  and unit tangent vector  $\mathbf{t}$  can be modeled using a simplified Young-Laplace-Equation (e.g. [7])

$$\mathbf{s} = \mathbf{n} \cdot \boldsymbol{\tau} = -p_{\text{ext}} \mathbf{n} - 2\gamma \kappa \mathbf{n} \quad (6)$$

$$\kappa = -\frac{1}{2} \cdot (\nabla_{\Gamma} \cdot \mathbf{n}); \quad \nabla_{\Gamma} = \nabla - n \partial_n = (\mathbf{I} - \mathbf{n} \mathbf{n}^T) \nabla \quad (7)$$

for constant  $\gamma$ . Therein the stress vector is denoted by  $\mathbf{s}$  and the external fluid only appears through its pressure  $p_{\text{ext}}$ . The surface gradient operator  $\nabla_{\Gamma}$  defines the mean curvature  $\kappa$  of the free surface. For a planar surface ( $\kappa = 0$ ) equation **Error! Reference source not found.** can be simplified to the free-slip boundary condition with fixed pressure if the wall is additionally claimed to be impermeable:

$$\mathbf{u} \cdot \mathbf{n} = 0; \quad \mathbf{s} \cdot \mathbf{n} = -p_{\text{ext}}; \quad \mathbf{s} \cdot \mathbf{t} = 0. \quad (8)$$

For arbitrarily shaped interfaces the normal component of the velocity is not necessarily zero. Thus, the interface has to be moved accordingly while still ensuring its impermeable nature. In the scope of our work the Arbitrary Lagrangian-Eulerian (ALE) technique was chosen to realize the interface tracking [8]. In simplified terms, the essential idea of ALE for free surface flows is to allow the grid - which is used for discretization - to move independently from the fluid flow. Only the free surface is under constraint, such that the fluid velocity  $\mathbf{u}$  equals the mesh velocity  $\mathbf{u}_m$  there. For all other boundaries  $\mathbf{u}_m$  is restricted accordingly. The independent mesh-movement away from the boundaries then allows a free and preferably smooth mesh point distribution. In our case a Laplace-smoothing for  $\mathbf{u}_m$  was utilized [9]. Stationary walls were modelled with the no-slip boundary condition ( $\mathbf{u} = \mathbf{0}$ ), whereas for the moving substrate wall an inhomogeneous Dirichlet boundary condition was necessary ( $\mathbf{u} = u_s \cdot \mathbf{e}_y$ , process direction  $y$ ). Along the wetted walls, the interface contact line may have the freedom to slide. Thus, the velocity must not be restricted there directly. To model this behavior, the generalized Navier-Slip boundary condition was consulted [10]:

$$\mathbf{u} \cdot \mathbf{n} = 0; \quad \mathbf{s} \cdot \mathbf{t} = -\frac{\eta}{\beta} \mathbf{u} \cdot \mathbf{t}. \quad (9)$$

The slip length  $\beta$  is present to relate a tangential boundary friction force to the current local slip velocity. For all of our calculations  $\beta = 0.01 \cdot h$  was used, where  $h$  denotes a mean local mesh (element) size of the discretized numerical model.

### 3. Simulation results

The basis of our analysis was to gain detailed information of all involved fields. To reduce the computational effort, we thought of the melt domain to be fixed during this first step: The magnetic field calculations including the Lorentz force were performed using the finite element solver OPERA (Cobham plc). The results revealed

high amplitudes for  $f$  in all regions close to edges and corners of the fluid domain as shown in Figure 2 (left).

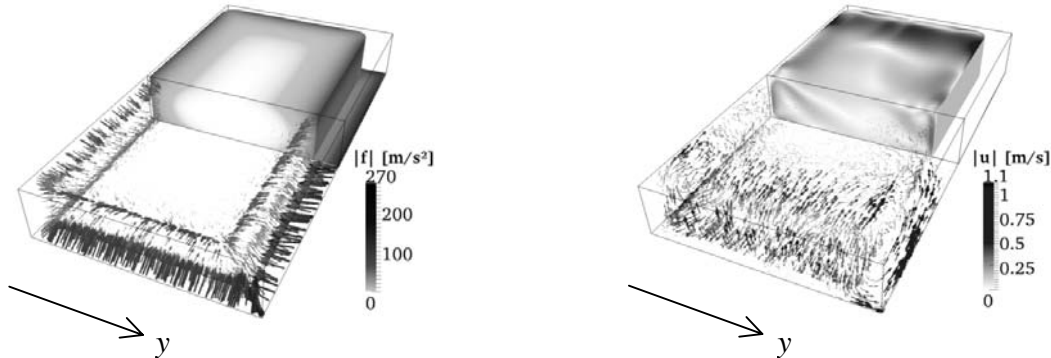


Figure 2: Lorentz-Force (left) and instantaneous velocity field (right) for a fixed fluid domain: In both figures all solid material domains are hidden. The front part shows the related vectors, the rear part the corresponding amplitudes for one half of the fluid domain, respectively. The process direction is indicated by  $y$ .

Given this, we concluded that the liquid silicon melt would actually be subject to a strong deformation if we had not restricted our model as a premise. The corresponding forced fluid flow was simulated with a finite volume

solver of the openFOAM library suite. The resulting velocity field  $u$  is also illustrated in Figure 2 (right) for comparison. That the fluid flow is mainly influenced by the Lorentz force is one substantial finding here. A boundary driving effect of the moving substrate along the  $y$ -direction can barely be identified since the global maximum velocity magnitude is more than one order of magnitude higher than  $u_s$ . Hence we assume that the magnetic force is mainly responsible for exciting flow instabilities. As the strong Lorentz force is however crucial to balance the gravitational force, it cannot simply be reduced. This can be demonstrated with

the help of the magnetic pressure  $p_B = \frac{B^2}{2\mu_0}$ .

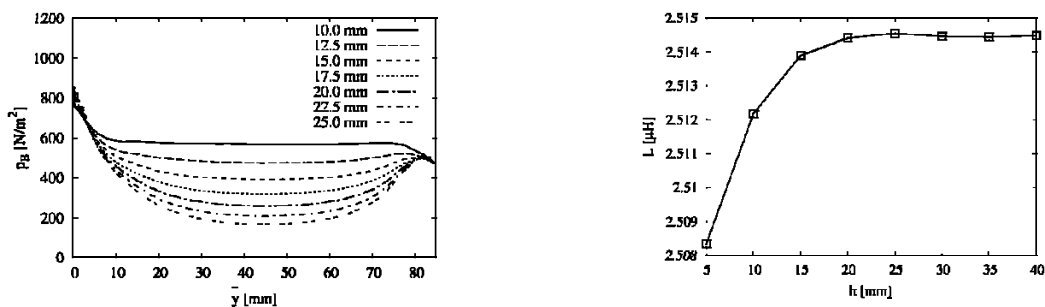


Figure 3: Magnetic pressure along a wafer side (left, arc length  $\bar{y}$ ) for different casting frame side wall strengths (Front:  $\bar{y} = 0\text{mm}$ , Back:  $\bar{y} \approx 78\text{mm}$ ) and magnetic inductivity (right) based on  $I_{RMS}$  for diff. melt heights.

Figure 3 (left) illustrates  $p_B$  along a wafer side for different casting frame side wall thicknesses as a result of an investigation on how the melt flow could be shielded in order to reduce the magnetic forcing on the bulk region. The hydrostatic pressure at the bottom of the

casting frame results in  $P_B = \rho g h \approx 506 \frac{\text{N}}{\text{m}^2}$  for a typical fixed melt level height of  $h = 20 \text{ mm}$ . Comparing  $P_B$  with the trends in Figure 3 (left) clearly shows that a properly working magnetic valve is very sensitive to small geometric changes. Figure 3 (right)

moreover shows the total magnetic inductivity  $L = \frac{W}{I_{\text{RMS}}^2}$  of the system against different melt

level heights, where  $W$  denotes the time-averaged magnetic field energy  $W = \frac{1}{2} \int (\mathbf{H} \cdot \mathbf{B})_z dV$ .

The total system inductivity proved not to be as sensitive as expected for measuring the melt level height based on phase or frequency shifts in the power supply of the excitation coil.

There is only a small change of just about 0.3% for  $L$  in the range of  $h = 5 \text{ mm}$  and  $h = 40 \text{ mm}$ . Further investigations will show if this is enough to produce a significant influence on the driving oscillating circuit. Recent development engaged in revising our model to account for surface deformation at the top of the fluid domain. Latest results for a successful 2D-simulation with COMSOL Multiphysics are presented in Figure 4.

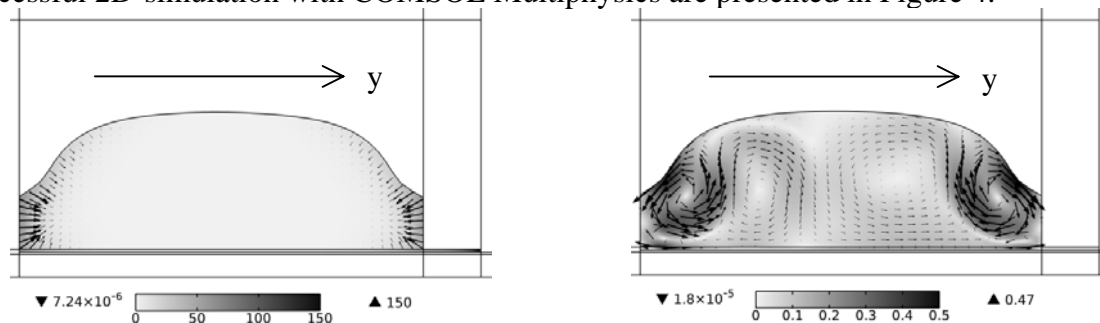


Figure 4: Dome shaping of the fluid domain for a simplified 2D-model (central longitudinal section of the 3D-model): Time-averaged Lorentz force (left) and fluid velocity (right) at the simulation time of  $t = 3 \text{ s}$  after applying the magnetic field.

The magnitudes of the Lorentz force (left) and the velocity field (right) are in quite good agreement with central longitudinal section of the 3D-model. From the shape of the dome and based on the maximum field magnitudes, this shows a manifold flow character and that none of the momentum source terms in equation **Error! Reference source not found.** is clearly dominating. This is one major reason which makes the whole modeling challenging and simulations require high computational costs, especially in 3D. But it also shows the dominance of the magnetic forcing compared to the driving effect of the moving substrate.

#### 4. Conclusion

The RGS process is a promising technology for future silicon wafer production, but the involved physics make high demands on numerical investigations which are necessary for improving process controllability and stability. We have successfully performed 3D-simulations to numerically confirm the functioning melt retention based on tailored magnetic fields. A parameter study revealed the total system inductivity as a function of the melt level. Finally, we demonstrated that the surface deformation is substantially important for a satisfactory model. Further investigations will mainly concern an improved contact line modelling, expected surface oscillations and the surface deformation in 3D.

**Acknowledgements.** Financial support for this research from the German Helmholtz Association in frame of the Alliance “Liquid Metal Technologies (LIMTECH)” is gratefully acknowledged.

## References

- [1] Schönecker, A., Geerligs, L. J., and Müller, A. *Solid State Phenomena*, 95-96 (2004), 149-158.
- [2] Hahn, G. and Schönecker, A. *Journal of Physics: Condensed Matter*, 16 (2004), R1615-R1648.
- [3] Santara, F., Delannoy, Y., and Autruffe, A. *Journal of Crystal Growth*, 340 (2012), 41-46.
- [4] Binns, K. J., Lawrenson, P. J., and Trowbridge, C. W. *The Analytical and Numerical Solution of Electric and Magnetic Fields*. Wiley, 1992.
- [5] Morisue, T. *IEEE Transactions on Magnetics*, 18 (1982), 531-535.
- [6] Ferziger, J. H. and Peric, M. *Computational Methods for Fluid Dynamics*. Springer-Verlag, 2002.
- [7] Scardovell, R. and Zalesk, S. *Annual Review of Fluid Mechanics*, 31 (1999), 567-603.
- [8] Hughes, T. J.R., Liu, W. K., and Zimmermann, T. K. *Computer Methods in Applied Mechanics and Engineering*, 29 (1981), 329–349.
- [9] COMSOL 4.4 Multiphysics Reference Manual. 2014.
- [10] Bruus, H. *Theoretical Microfluidics*. Oxford University Press, 2008.